

## Kinetics of capillary wetting in nanoporous films in the presence of surface evaporation

Erkin Seker, Matthew R. Begley, Michael L. Reed, and Marcel Utz

Citation: [Applied Physics Letters](#) **92**, 013128 (2008); doi: 10.1063/1.2831007

View online: <http://dx.doi.org/10.1063/1.2831007>

View Table of Contents: <http://scitation.aip.org/content/aip/journal/apl/92/1?ver=pdfcov>

Published by the [AIP Publishing](#)

---

### Articles you may be interested in

[Biphilic nanoporous surfaces enabled exceptional drag reduction and capillary evaporation enhancement](#)  
Appl. Phys. Lett. **105**, 191611 (2014); 10.1063/1.4901962

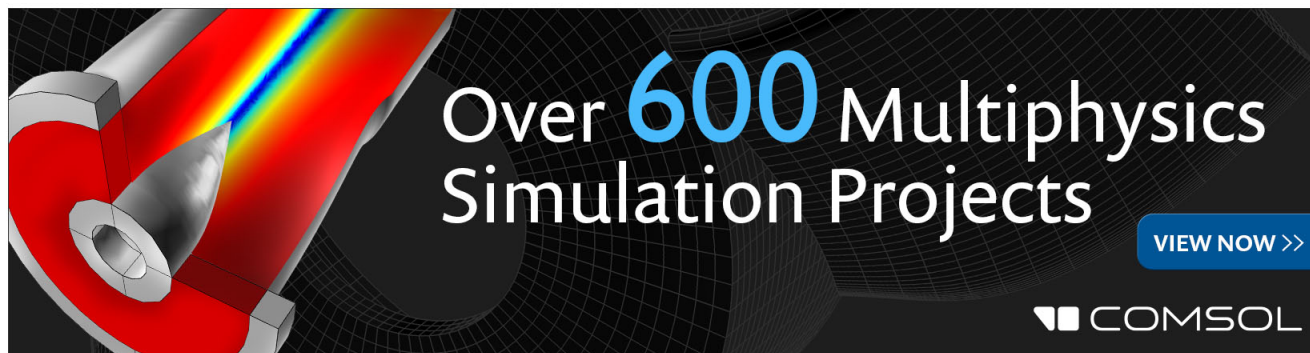
[On the localized surface plasmon resonance modes in nanoporous gold films](#)  
J. Appl. Phys. **115**, 044308 (2014); 10.1063/1.4862440

[Evaporation of sessile droplets on nano-porous alumina surfaces](#)  
AIP Conf. Proc. **1547**, 156 (2013); 10.1063/1.4816864

[On the effect of surface roughness height, wettability, and nanoporosity on Leidenfrost phenomena](#)  
Appl. Phys. Lett. **98**, 083121 (2011); 10.1063/1.3560060

[Wetting kinetics of a thin film evaporating in air](#)  
Phys. Fluids **19**, 112104 (2007); 10.1063/1.2815737

---

The advertisement features a dark background with a grid pattern. On the left, there is a 3D simulation of a mechanical part with a red and yellow color gradient. The text "Over 600 Multiphysics Simulation Projects" is prominently displayed in the center. Below this text, there is a blue button with the text "VIEW NOW >>". In the bottom right corner, the COMSOL logo is visible, consisting of a small square icon followed by the word "COMSOL".

# Kinetics of capillary wetting in nanoporous films in the presence of surface evaporation

Erkin Seker

Department of Electrical and Computer Engineering and Department of Chemistry, University of Virginia, Virginia 22904, USA

Matthew R. Begley

Center For Microsystems For The Life Sciences, Department of Mechanical and Aerospace Engineering, and Department of Materials Science and Engineering, University of Virginia, Virginia 22904, USA

Michael L. Reed

Center For Microsystems For The Life Sciences and Department of Electrical and Computer Engineering, University of Virginia, Virginia 22904, USA

Marcel Utz<sup>a)</sup>

Center For Microsystems For The Life Sciences and Department of Mechanical and Aerospace Engineering, University of Virginia, Virginia 22904, USA

(Received 11 November 2007; accepted 13 December 2007; published online 10 January 2008)

A liquid in contact with a nanoporous Au film forms a halo of constant width around the droplet. Due to the large surface area-to-volume ratio, one would expect either complete wetting or rejection of the liquid. Instead, a stable halo width is observed, depending on pore size, void fraction, film thickness, and the liquid. This is due to competition between capillary flow and evaporation through the surface of the nanoporous film. A theory is presented that predicts the halo width from the film geometry and liquid properties. Without adjustable parameters, the theory is in good agreement with experimental results. © 2008 American Institute of Physics. [DOI: 10.1063/1.2831007]

Nanoporous gold (np-Au) is a versatile material for sensor and catalyst applications due to its relatively high surface-to-volume ratio, electrical conductivity, and chemical inertness. One way to produce np-Au is to selectively dissolve (dealloy) the less noble constituent of a gold-based alloy.<sup>1</sup> Recent studies focused on the structure-property relationships of np-Au (Refs. 2–4) and developed various sensors<sup>5–7</sup> and catalysts.<sup>8</sup> The objective of this paper is to highlight an interesting wetting phenomenon, where a liquid drop placed on a flat nanoporous gold film produces a wetting halo, as seen in Fig. 1. This phenomenon is not observed on compact gold films. According to a simple thermodynamic equilibrium model based on the contact angle of a liquid dispensed on the np-Au surface, the liquid should either wet the pore matrix completely or be expelled from the surface. However, the experimental observation suggests an intermediate situation, where the liquid wets the porous structure to a stable distance which is not affected by the droplet size.

While the width of this wetting halo is stable as long as the sample is exposed to the laboratory air, covering it with a petri dish immediately causes the halo to grow. This provided an experimental indication that the phenomenon is related to evaporation, and motivated the development of a model that includes its effect. As will be shown, this model matches experimental data without any adjustable parameters.

The geometry of the problem is laid out in Fig. 1. A nanoporous film with surface area-to-volume ratio  $\rho$ , void fraction  $\beta$ , and thickness  $h$  is in contact with a liquid droplet.

The difference in surface energy between solid-air and solid-liquid interface is given by<sup>9</sup>

$$\Delta\gamma = \gamma_{\text{solid-air}} - \gamma_{\text{solid-liquid}} = \gamma \cos \theta, \quad (1)$$

where  $\gamma$  is the surface tension of the liquid and  $\theta$  is the contact angle.  $\Delta\gamma$  corresponds to the free energy gain per wetted surface area. Through capillary action, a front of the liquid advances from the edge of the droplet into the film. We will assume the liquid edge to be a straight line perpendicular to the  $x$  direction. In this way, the problem becomes one dimensional. The position of the advancing liquid front in the porous film is designated by  $x_m$ .

We assume that the liquid evaporates from the free surface of the porous film at a rate  $q$ , defined by the volume of

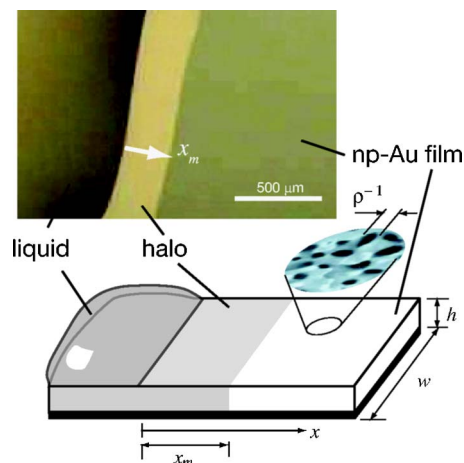


FIG. 1. (Color online) Micrograph (top) and schematic (bottom) of the wetting halo forming around a liquid droplet sitting on top of a thin film of nanoporous Au.

<sup>a)</sup> Author to whom correspondence should be addressed. Electronic mail: marcelutz@virginia.edu.

liquid evaporating per unit of time per unit of exposed surface area. In general,  $q$  will be a function of the difference between the actual and the saturation vapor pressure of the liquid species in the atmosphere above the film, the shape of the pores, the void fraction, and the temperature. Also note that the saturation vapor pressure of a liquid in a porous medium is typically lower than that of the bulk.<sup>10</sup>

Under isothermal conditions, the heat of vaporization is continuously supplied by heat transport from the substrate. This is a reasonable assumption for films of only a few microns supported on a silicon wafer of several millimeter thickness. The condition of continuity leads to

$$h\beta v'(x, t) + q = 0, \quad (2)$$

where  $v(x, t)$  is the velocity of the liquid in the  $x$  direction, averaged through the thickness of the film, and  $\beta$  is the void fraction. The mechanical power  $dW_{\text{mech}}$  acting on a segment  $dx$  of the wet part of the film is given by

$$dW_{\text{mech}} = (pv)' wh\beta dx, \quad (3)$$

where  $p = p(x, t)$  is the pressure in the liquid phase. At the same time, the evaporation on the surface of the segment  $dx$  dries out a portion of the nanoporous film which is continuously re-wetted. This leads to an additional driving force for flow, with a differential power of

$$dW_{\text{et}} = \rho\Delta\gamma\beta^{-1}qwdx. \quad (4)$$

These two power terms must balance the loss due to viscous drag in the system. In order to estimate the viscous power dissipation, we assume the pores to be hollow cylinders with their axes aligned with the  $x$  direction, and their diameter given by the inverse of the surface area-to-volume ratio  $\rho$ . Due to the small scale of the pores and the low flow velocities, we can safely assume the flow to be fully laminar, and use the Hagen-Poiseuille expression. The result will differ from the actual power dissipation by a factor of order unity representing the specific morphology of the pores. One obtains

$$dW_{\text{sc}} = 8\eta\rho^2v^2(x, t)wh\beta dx, \quad (5)$$

where  $\eta$  is the viscosity. Balancing power, one finds

$$(pv)' + 8\eta\rho^2v^2 + q\rho\Delta\gamma(h\beta) = 0. \quad (6)$$

The problem consists of finding a velocity and a pressure profile that solve both Eqs. (2) and (6), while satisfying suitable boundary and initial conditions. The continuity equation can be integrated immediately to give

$$v(x, t) = C(t) - qx(h\beta). \quad (7)$$

The constant of integration is found by noting that any liquid passing through  $x=0$  must either evaporate or lead to an advance of the position of the wetting front  $x_m$ . This gives

$$\beta h w v(0, t) = q w x_m(t) + h w \beta \dot{x}_m(t). \quad (8)$$

The velocity profile is, therefore,

$$v(x, t) = \dot{x}_m(t) + q(h\beta)[x_m(t) - x]. \quad (9)$$

In the special case of vanishing evaporation rate,  $q=0$ , the velocity profile is constant over  $x$ , and Eq. (6) simplifies to

$$8\eta\rho^2v(t) = -p', \quad (10)$$

as expected in laminar, conservative flow. Since the left hand side of this equation is purely a function of time, the pressure gradient must be constant as function of  $x$ .

At the advancing edge, the pressure in the liquid is lowered by the wetting energy. This provides the boundary condition

$$p(x_m, t) = p(0, t) - \Delta\gamma\rho. \quad (11)$$

In the absence of evaporation ( $q=0$ ), the position of the advancing edge can be found from this by inserting Eq. (10) into Eq. (9), and integrating the resulting differential equation, to obtain

$$x_m^0(t) = 12\sqrt{t\Delta\gamma(\rho\eta)}, \quad (12)$$

where we have assumed  $x_m(t=0)=0$ , and the superscript indicates the case of vanishing evaporation rate. No steady-state solution exists for  $q=0$ ; the wetting front will continue to advance as long as there is a supply of liquid left, albeit at an ever decreasing rate.

If  $q > 0$ , a steady-state solution can be found by requiring that  $\dot{x}_m(t)=0$ . The velocity profile then becomes

$$v_{\text{ss}}(x) = q(h\beta)(x_m^{\text{ss}} - x). \quad (13)$$

The steady-state position of the wetting front  $x_m^{\text{ss}}$  can be found by introducing Eq. (13) into Eq. (6). The resulting differential equation for  $p(x)$  is easily integrated to yield the pressure profile

$$p(x) = \frac{8\eta\rho^2q}{h\beta}x^2 - \left(\frac{\Delta\gamma\rho}{x_m^{\text{ss}}} + \frac{8\eta\rho^2x_m^{\text{ss}}}{h\beta}\right)x. \quad (14)$$

The steady-state location of the wetting front is found from requiring that  $p'(x_m^{\text{ss}})=0$ . This yields

$$x_m^{\text{ss}} = \sqrt{\frac{h\beta\Delta\gamma}{8\eta\rho q}}. \quad (15)$$

In order to test this result experimentally, several parallel  $1.5 \times 40 \text{ mm}^2$  rectangles of silver-gold ( $\text{Au}_{0.4}\text{Ag}_{0.6}$ ) alloy were photolithographically patterned on 50 mm diameter silicon wafers. Film thicknesses of 200, 400, and 600 nm were obtained by sputter coating wafers for different deposition durations. Each wafer was then scribed with a dicing saw to produce 18 individual chips, each containing a  $1.5 \times 20 \text{ mm}^2$  AuAg rectangle, but not yet broken into individual pieces until after dealloying. The AuAg films were dealloyed by immersing the wafers in nitric acid at 95 °C for 10 min, followed by rinsing in de-ionized (DI) water, and drying under  $\text{N}_2$ . For each film thickness, some of the samples were used in this form, and some were annealed at 150 °C and some at 200 °C for 10 min under  $\text{N}_2$  at atmospheric pressure. This step increases the pore size and slightly decreases void fraction, widening the range of different morphologies available for experiments.<sup>2</sup> In summary, this procedure produced two identical samples for each film thickness and annealing state. The final film thickness was measured using a stylus-based profilometer with a stylus force of 10  $\mu\text{N}$ . Void fraction and pore dimensions were determined by image analysis of scanning electron micrographs.<sup>2,11</sup> The results were  $\beta = 32 \pm 4\%$ ,  $\rho =$

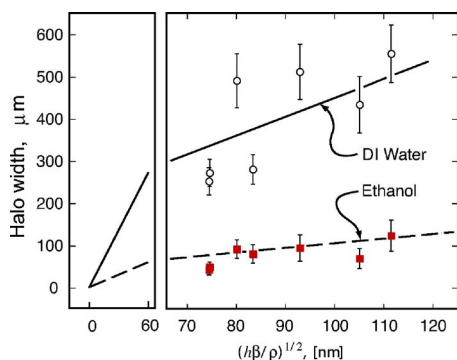


FIG. 2. (Color online) Experimentally measured halo width values are plotted with respect to the product of film thickness  $h$ , void fraction  $\beta$ , and pore diameter  $\rho^{-1}$ . The lines have been calculated from  $x_m^{ss} = \sqrt{h\beta\Delta\gamma 8\eta\rho q}$  Eq. (15) without adjusting any parameters, using literature values for the viscosity and surface energy, and measured values of film thickness, pore size, and void fraction.

$=33 \pm 11$  nm without annealing,  $\beta = 32 \pm 3\%$ ,  $\rho^{-1} = 37 \pm 10$  nm for films annealed at  $150^\circ\text{C}$ , and  $\beta = 37 \pm 3\%$ ,  $\rho^{-1} = 57 \pm 8$  nm for films annealed at  $200^\circ\text{C}$ .

Immediately prior to the wetting experiments, each sample was cleaned for 3 min at a power of 100 W in a March PX-250 plasma oxidizer. The samples were then dipped in petri dishes of ethanol (Fluka, puriss.) or DI water (Millipore), and the drying process was observed under a stereoscopic microscope. A digital video camera was attached to the microscope to record the wetting halo. All experiments were carried out at a room temperature of  $25 \pm 0.5^\circ\text{C}$  and a relative humidity of  $(60 \pm 5)\%$ . For each sample, the halo width was measured ten times at various locations and video frames using a screen-ruler software.

Figure 2 shows the experimental halo width as a function of  $(h\beta\rho)^{1/2}$  for ethanol (filled squares) and DI water (open circles). Each data point represents three different samples, and ten individual measurements. The error bars are standard deviations. Clear trends are visible; the halo widths for ethanol are about five times smaller than for water, and there is a clear correlation with the geometric parameter  $(h\beta\rho)^{1/2}$ , in spite of considerable scatter in the data. Figure 2 contains data points for all samples tested, with the exception of the combination of largest thickness (600 nm) and annealing at  $200^\circ\text{C}$ , which did not show any wetting halo at all. It is known that annealing of thick layers causes not only pore size growth, but leads to profound changes in morphology. Scanning electron microscopy (SEM) micrographs of these films exhibit large cracks (not shown). It is possible that the network of pores is no longer sufficiently contiguous at this point to allow the liquid to penetrate.

The model predictions are shown by solid and dashed lines in Fig. 2. It is important to note that no adjustable parameters were fitted to the data. Rather, the lines were calculated directly from Eq. (15). The required values for the evaporation rates  $q$  of ethanol and DI water ( $0.12$  and  $0.026 \mu\text{m s}^{-1}$ ) were determined by measuring the weight loss due to evaporation from a petri dish on a microbalance. Wetting energies  $\Delta\gamma$  were obtained for ethanol and DI water ( $1.17$  and  $3.81 \text{ mJ m}^{-2}$ ) using a contact angle of  $87^\circ$ , typical for water on gold surfaces,<sup>12</sup> and surface tensions of  $72.75 \text{ mJ m}^{-2}$  for water and  $22.39 \text{ mJ m}^{-2}$  for ethanol.<sup>13</sup> The viscosities of ethanol and DI water ( $8.9 \times 10^{-4}$  and  $10.7$

$\times 10^{-4} \text{ N s m}^{-2}$ ) were also taken from the literature.<sup>14</sup>

Within the statistical variation of the experimental observations, the predicted halo widths agree with the observed ones. Therefore, we conclude that the model captures the essential physical basis of the observed phenomenon. The remaining scatter of the data may be due to a number of factors. The pore size was varied by annealing. This, however, is known to not only increase the size of the pores, but also change their morphology. In terms of the theory laid out here, this is expected change the prefactor that relates the viscous drag to the pore size. On the other hand, the theory has been developed for a straight wetting line, neglecting curvature effects. The data presented here have not been selected according to the curvature of the wetting line. Finally, there may be some scatter due to variability of pore morphology and Au surface contamination from one sample to the next.

Variations in evaporation rate at the time of observation due to air currents and different conditions of temperature and humidity are also likely to contribute to the scatter in the data. Another limitation is that the evaporation rate was taken as a constant in the halo width calculations; however, it is in fact a function of film morphology. Mudcracks are known to form in thicker films as a result of tensile stress accumulation during annealing, and are readily observed in SEM micrographs. These cracks may function as pathways that facilitate evaporation from deeper layers of the film. This may explain that no halo was observed in the case of the thickest films annealed at  $200^\circ\text{C}$ .

In conclusion, capillary wetting in nanoporous Au films has been observed to form a stable halo saturated with liquid around the droplet sitting on top of the film. The width of this halo is determined by the competition between capillary transport through the film and evaporation of the liquid through the surface. A simple transport theory developed on the basis of this model predicts wetting halo widths that are in quantitative agreement with experimental observations.

We gratefully acknowledge the support of the National Science Foundation through Grants DMI-0507023 and DMR-0647790.

- <sup>1</sup>J. Erlebacher, M. J. Aziz, A. Larma, N. Dimitrov, and K. Sieradzki, *Nature* (London) **410**, 450 (2001).
- <sup>2</sup>E. Seker, J. T. Gaskins, H. Bart-Smith, J. Zhu, M. L. Reed, G. Zangari, R. G. Kelly, and M. R. Begley, *Acta Mater.* **55**, 4593 (2007).
- <sup>3</sup>A. M. Hodge, J. Biener, J. R. Hayes, P. M. Bythrow, C. A. Volkert, and A. V. Hamza, *Acta Mater.* **55**, 1343 (2007).
- <sup>4</sup>D. Lee, X. Wei, X. Chen, M. Zhao, S. Jun, J. Hone, E. G. Herbert, W. C. Oliver, and J. W. Kysar, *Scr. Mater.* **56**, 437 (2006).
- <sup>5</sup>M. Hieda, R. Garcia, M. Dixon, T. Daniel, D. Allara, and M. H. W. Chan, *Appl. Phys. Lett.* **84**, 628 (2004).
- <sup>6</sup>Z. Liu and P. C. Searson, *J. Phys. Chem. B* **110**, 4318 (2006).
- <sup>7</sup>N. V. Lavrik, C. A. Tipple, M. J. Sepaniak, and P. G. Datskos, *Biomed. Microdevices* **3**, 35 (2001).
- <sup>8</sup>R. Zeis, A. Mathur, G. Fritz, J. Lee, and J. Erlebacher, *J. Power Sources* **165**, 65 (2007).
- <sup>9</sup>P. G. de Gennes, *Rev. Mod. Phys.* **57**, 827 (1985).
- <sup>10</sup>R. Evans, U. Marini Bettolo Marconi, and P. Tarazona, *J. Chem. Phys.* **84**, 2376 (1986).
- <sup>11</sup>U. National Institute of Health, Wcif imagej 1.37a.
- <sup>12</sup>M. Yekta-Fard and A. B. Ponter, *Phys. Chem. Liq.* **15**, 19 (1985).
- <sup>13</sup>G. W. C. Kaye and T. H. Laby, *Tables Of Physical And Chemical Constants*, 16th ed. (Harlow, Essex, 1995).
- <sup>14</sup>D. R. Lide, *Handbook of Chemistry and Physics*, 73rd ed. (CRC, Boca Raton, 1994).